Sustainable Energy & Fuels

Accepted Manuscript

This article can be cited before page numbers have been issued, to do this please use: J. Cao, L. Li, Y. Xi, J. Li, X. Pan, D. Chen and W. Han, *Sustainable Energy Fuels*, 2018, DOI: 10.1039/C8SE00123E.

ROYAL SOCIETY OF CHEMISTRY

rsc.li/sustainable-energy

View Article Online
DOI: 10.1039/C8SE00123E

Journal Name

ARTICLE

Core-shell structural PANI-Derived Carbon@Co-Ni LDH electrode for high-performance asymmetric supercapacitors

Received 00th January 20xx,
Accepted 00th January 20xx

DOI: 10.1039/x0xx00000x

www.rsc.org/

Junming Cao,[a] La Li,[a] Yunlong Xi, [c] Junzhi Li,[a] Xuexue Pan,[a] Duo Chen,[a] and Wei Han *[ab]

Carbon/metal nanocomposites have been considered as a promising electrode material for application in supercapacitors owing to the combination of good electrical conductivity, excellent cycle stabilities of electronic double layer capacitor (EDLC) and high specific capacitance of pseudocapacitor. Here, a core-shell structured polyaniline derived carbon nanowire @ Co-Ni layered double hydroxide (PANC@Co-Ni LDH) nanomaterials were successfully synthesized via a novel facile electrodeposition-carbonization-electrodeposition route. The core-like PANC full of N atom remains innate long-chain structure and provides a lot of active sites for the uniform growth of the shell-like Co-Ni LDH, resulting in a cross-linked active network structure with numerous electroactive sites, abundant pore, adequate large space and reaction interface, which contribute to the rapid diffusion and transportation of the electrolyte ions and electrons. Therefore, as-obtained PANC@Co-Ni LDH showed a high specific capacitance of 1529.52 F g^{-1} at 0.5 A g^{-1} in three electrode system and offered an outstanding rate properties with no obvious capacitance attenuation (1425.17 F g^{-1}) when the current density increased up to 10 A g^{-1}. Moreover, the asymmetric supercapacitor using PANC@Co-Ni LDH as the positive electrode and PANC as the negative electrode were fabricated, which revealed a high specific capacitance of 214.28 F g^{-1} and superior energy density of 38.73 W h kg^{-1} with a power density of 0.92 kW kg^{-1}, suggesting great potential in practical energy storage devices.

Introduction

In recent years, supercapacitors (SCs) as eco-friendly energy storage device have been widely applied to electronics, mobile electrical systems, energy management, memory back-up systems, and industrial power arrays due to its advantages such as long service life, rapid charge/discharge rate and high power density.[1-4] Typical SCs are usually consisted of electrode materials, electrolyte, separator and current collector. Most closely related to the electrochemical performance improvement of SCs, are the optimization and development electrode materials, which can be divided into four categories of carbon materials,[5-7] conducting polymer,[8-10] metal oxide[11-15] and composites. Among them, composites have attracted more attentions because of the complementary advantages of various electrode materials. Carbon materials/metal nanocomposites that possess excellent cycling properties of carbon materials and high specific capacitance of metal oxide have been widely studied as the best partners.

In the carbon materials/metal system,[16-18] the extremely hot choice of carbon materials belongs to the one-dimensional (1D) carbon nanotube (CNTs)[19] and multiwall carbon nanotubes (WMCNTs) due to their higher length-diameter ratio and better electrical conductivity in comparison with 2D graphene, carbides and nitrides (MXene)[20-22] etc. However, CNTs or MWCNTs are usually synthesized through a sophisticated method like chemical vapor deposition (CVD)[23, 24] and the obtained CNTs with highly crystalline need extra treatment (like acid-oxidation) to generate some functional groups such as hydroxyl and carboxyl[25] on the surface aiming at easy and efficient combination with metal oxides. Alternatively, conducting polymer like PANI could be directly transformed to a novel kind of carbon materials after one-step direct carbonization process, which remains the original 1D nanowires structure and offers more active sites compared to CNT. Remarkably, the PANI-derived carbon (PANC) is rich in N atoms,[26-29] facilitating electron conduction rate, materials activity (extra pseudocapacitance) and wettability. As to transition metal oxides, Co-Ni layered double hydroxide (Co-Ni LDH)[30-33] with high specific capacitance have been demonstrated as an outstanding PSC material for SCs because of the common effect of binary redox states (Ni^{2+}/Ni^{3+} and Co^{2+}/Co^{3+} couples) and the unique layered crystal structure, which could reduce the difficulty of the electrolyte ions diffusion among electrode materials. Based on the above considerations, in this paper, we have successfully prepared core-shell structured PANI-derived carbon/Co-Ni LDH

[a] The Engineering Laboratory of Supercapacitor (Jilin Province), College of Physics, Jilin University, Changchun, 130012, PR China. E-mail: whan@jlu.edu.cn.
[b] International Center of Future Science, Jilin University, Changchun City 130012, PR China.
[c] School of Physics and Electronic Engineering, Linyi University, PR China
† Footnotes relating to the title and/or authors should appear here.
Electronic Supplementary Information (ESI) available: [details of any supplementary information available should be included here]. See DOI: 10.1039/x0xx00000x

View Article Online
DOI: 10.1039/C8SE00123E

(PANC@Co-Ni LDH) nanocomposite. The obtained electrode material showed excellent rate capability with a slight capacitance loss of 10% as the current density increased by 20 times. Moreover, in order to enlarge the voltage window and realize its practical application, the asymmetric supercapacitor (ASC) was assembled by the negative PANC electrode and the positive PANC@Co-Ni LDH electrode, respectively. The fabricated ASC devices exhibited excellent cycle stability with a capacitance retention of 84.73% even after 10,000 charge-discharge tests at a large voltage range of 0~1.4 V, providing an advanced electrode material for energy supply units.

Experimental

Materials

Carbon fiber paper (CFP) was purchased from SGL Technology Company. Sulfuric acid (98% H_2SO_4), Aniline (99.5%), $CoCl_2{\cdot}6H_2O$, $Ni(NO_3)_2{\cdot}6H_2O$ and KOH were purchased from Sinopharm Chemical Reagents and used without further purification. The CFP was cut into 1 × 2 cm^2 and cleaned with acetone and deionized (DI) water for several times to remove the surface oxide.

Synthesis of PAN-Carbon (PANC) NWs

Typically, The PANC materials were prepared via carbonization of the electrodeposited polyaniline (PANI). The electrodeposition process was performed in a three-electrode system with 60 ml 0.2 M H_2SO_4 solutions and 3 ml aniline as electrolyte, CFP as working electrode, Pt as the counter electrode and a saturated calomel electrode (SCE) as reference electrode. The PANI-x@CFP samples were obtained after deposition at scan rate of 100 mV s^{-1} for x (x=20, 25, 30, 35 and 40) cycles at room temperature. Then, as-prepared PANI-x@CFP were washed with DI water for several times and dried at 60 °C for 12 hours. After fully drying, PANI-x@CFP was put into a quartz tube and carbonized at 800 °C under nitrogen atmosphere for 2 h.

Synthesis of the PANC@LDH NWs

The PANC@Co-Ni LDH NWs materials were prepared by employing electrodeposition method in the aforementioned three-electrode system. The differences are that PANC-35 materials hold the post of working electrode and the electrolyte contains 50 mL of 0.15M $CoCl_2{\bullet}6H_2O$ and 0.15M $Ni(NO_3)_2{\bullet}6H_2O$. The electrodeposition was carried out at constant potential of –1.0 V for 100-400s. The final samples were denoted as PANC@ LDH-T (T=100, 200, 300, 400s). The electrochemical synthesis process of Co-Ni LDH was divided into two step:

(i) The reduction of NO_3^- on the working electrode

$$NO_3^- + H_2O + 2e^- \rightarrow NO_2^- + 2OH^- \quad (1)$$

(ii) The generated OH^- leads to the coprecipitation of Co-Ni LDH on the surface of PANC

$$Co^{2+} + Ni^{2+} + 4\ OH^- \rightarrow CoNi(OH)_4 \quad (2)$$

Fabrication of PANC@LDH//PANC Asymmetric Supercapacitors (ASC)

The ASC device was fabricated with LDH-300@PANCand PANC-35 (1×1 cm^2, respectively) as positive and negative electrodes, respectively, filter paper as the separator, and 6 M KOH as the electrolyte in a stainless steel CR2032 coin construction. The total active mass loading of the device is about 18.9 mg.

Materials characterization

The field emission scanning electron microscopy (FESEM, Magellan 400) equipped with an energy dispersive X-ray spectrometer (SEM-EDX, Magellan 400) and transmission electron microscopy (TEM, JEOL JSM-2010F) were used to characterize the morphology, microstructure and element compositions of as-fabricated samples. The X-ray diffraction (XRD) was measured by a Japan Rigaku 2550 X-ray powder diffractometer with Cu Kα radiation (λ = 1.54056 Å) operating at 40 kV and 250 mA. The surface chemical states of samples were investigated utilizing the X-ray photoelectron spectroscopy (XPS) measurement performed on a VG ESCALAB MK II electron spectrometer.

Electrochemical Measurements

The electrodeposition process was finished by employing CHI 760D electrochemical work station (CH Instruments Inc., Shanghai, China). The CV, GCD and EIS tests were carried out using an IVIUM (Netherlands) electrochemical working station at room temperature, and the cycling stability of the fabricated devices were tested by LAND CT21001A, respectively. The EIS were investigated by applying an AC voltage with 5 mV amplitude in a frequency range from 0.01 Hz to 100 kHz at open circuit potential.

The calculation of all devices was obtained according to our previous reports.[4]

Results and discussion

Structure and morphology characterization

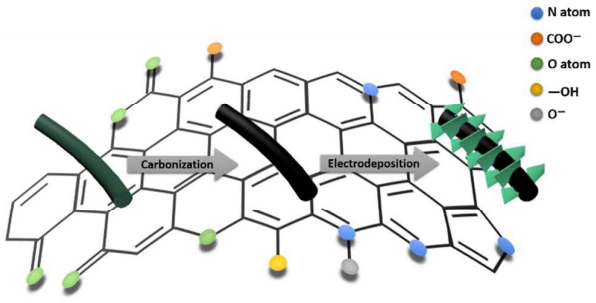

Scheme 1. Schematic illustration of the synthesis of PANC and PANC@LDH nanowires

The PANC@Co-Ni LDH core-shell nanostructured was synthesized by three steps, as illustrated in Scheme 1: (i) PANI nanowires array was deposited on carbon fiber paper (CFP) substrate by electrochemical polymerization method; (ii) PANI nanowires were carbonized to prepare the PAN-carbon (PANC); (iii) Co-Ni LDH directly grow on the surface of the PANC via

View Article Online
DOI: 10.1039/C8SE00123E

electrodeposition. CFP substrate was selected because of its good conductive and excellent flexiblity.[33] As-obtained PANC materials retain the nanowire structure of PANI perfectly and contain high levels of nitrogen/oxygen functional groups, which is beneficial for in-situ growth of Co-Ni LDH.

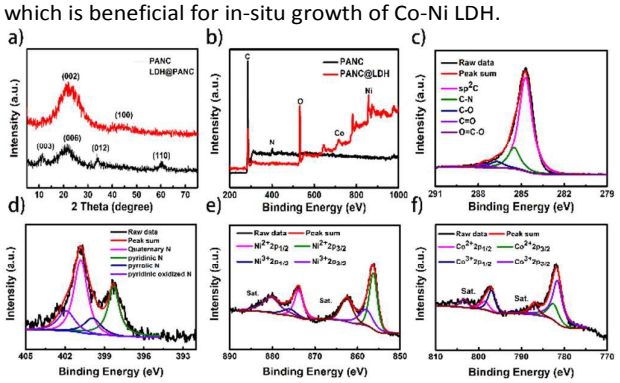

Fig. 1 Structural characterization of the prepared PANC-35 and PANC@Co-Ni-300 LDH samples: (a) XRD patterns; (b) XPS survey, (c) high-resolution C 1s spectra and (d) N 1s spectra of PANC samples; (e) high-resolution Ni 2p and (f) Co 2p spectra of PANC@Co-Ni LDH materials.

The X-ray diffraction pattern (XRD) measurements were conducted to characterize the crystal structure of the as-prepared hybrids (the PANC@Co-Ni LDH-300 and PANC-35 NWs), as shown in Fig. 1a. The two broad peaks located at about 23° and 43.7° for the PANC are corresponding to the (002) of the stacking graphene layers and (100) planes of the ordered graphitic structure. After coating with the Co-Ni LDH layer, the (003), (006), (012) and (110) planes that represent the Co-Ni LDH material were clearly observed, providing the successfully growth of the LDH shell with high crystallinity on the surface of the PANC NWs.

The prepared PANC-35 and PANC@Co-Ni LDH-300 samples then were characterized by X-ray photoelectron spectroscopy (XPS). Fig. 1b showed the XPS survey of these two simples. It can be clearly seen the existence of O, C, N elements in the PANC materials. The high-resolution O 1s spectra of the PANC (Fig. S1) can be deconvoluted into 4 peaks at 530.1, 532.3, 533.1 and 534.5 eV, corresponding to O-I(carbonyl oxygen of quinones), O-II(carbonyl oxygen atoms in esters, anhydrides, and oxygen atoms in hydroxyl groups), O-III(non-carbonyl (ether-type) oxygen atoms in esters and anhydrides) and O-IV(carboxylic groups with COOH or adsorbed water and/or oxygen). Subsequently, high-resolution C 1s and N 1s spectra of PANC was presented in Fig. 1b and 1c, respectively. The primary peak at 284.8 eV and weak peaks at 285.4 eV, 286.7 eV, 287.8 eV and 289.8 eV, corresponding to C=C and C-N, C-O, C=O, O=C-O bonds, can be observed. Depending on the position of N atoms in the carbon network, the high-resolution N 1s spectrum can be classified into quaternary N (400.6 eV), pyridinic N (398.2 eV), pyrrolic N (399.7 eV) and pyridinic oxidized N (402.4 eV),[34] providing that the N atom can be intactly retained after carbonization of PANI. That is to say, PANC can be served as one of the self N-doped carbon-based materials. Besides, the N, O elements on the PANC surface could enhance its wettability and conductivity in favor of transmission of electrolyte ions and electrons. The Ni 2p spectrum (Fig. 1e) showed two kinds of nickel peaks, where binding energy of 873.8 and 855.6 eV correspond to the Ni $2p_{1/2}$ and Ni $2p_{3/2}$ signals of (Ni^{2+}), peaks at 874.9 and 856.9 eV can be ascribed to Ni $2p_{1/2}$ and Ni $2p_{3/2}$ (Ni^{3+}). The deconvoluted spectrum of Co 2p (Fig. 1f) with binding energy of 797.5 eV and 782.1 eV can be attributed to Co $2p_{1/2}$ and Co $2p_{3/2}$ (Co^{2+}) and 795.4 and 780.5 eV can be ascribed to the Co $2p_{1/2}$ and Co $2p_{3/2}$ (Co^{3+}), suggesting the successful synthesis of Co-Ni LDH in the nanocomposites.

Fig. 2a and 2b showed the FESEM images of the PANI-35 and PANC-35. The PANI nanowires (Fig. 2a) homogeneously grow on the surface of CFP with a three-dimensional cross-linked network. It is noteworthy that after carbonization at 800 °C for 2 h, PANC materials remain slender interwoven nanowires morphology, which benefits to rapid electron-conduction, the XRD patterns also indicate the PANI nanowires were utterly carbonized to PANC (See Fig. S9). Fig. S2 showed the SEM images of PANC-20, PANC-25 and PANC-30, the length of PANC nanowires are shorter than that of PANC-35, when electrodeposition time increased to 40 cycles, the length grew longer and the mass loading on the CFP increased to 7.8 mg compared to PANC-35 (Fig. S3), then the accumulation of carbon fibers appeared, which impedes the passage of ions and reduces specific capacitance. Therefore, the following experiments we chose PANC-35 as template to electrodeposited Co-Ni LDH nanosheets.

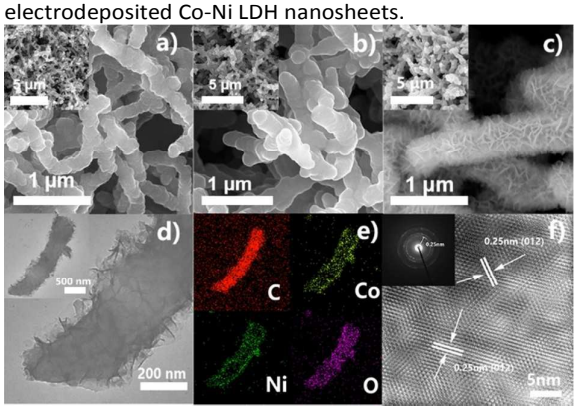

Fig. 2 (a-c) FESEM images of the obtained PANI-35, PANC-35, PANC@ Co-Ni LDH-300 sample; (d, e) TEM images of PANC@Co-Ni LDH with the corresponding elemental mapping images of C, Co, Ni and O elements; (f) FFT image of PANC@Co-Ni LDH-300, the inset is SAED pattern.

In order to obtain the optimum electrodeposition time (T) for Co-Ni LDH, we performed contrast test (T=100, 200, 300, 400s). The SEM with different T in Fig. S4 revealed the amount of Co-Ni LDH increase as T rising, the typical nanoflakes structure of Co-Ni LDH has not universally formed under 100s and that is too many even beginning to aggregation under 400s. Based on this, sample PANC@Co-Ni LDH-300 was further investigated, as shown in Fig. 2c-2f. Co-Ni LDH aligned vertically on the PANC can be found from Fig. 2c and 2d. The corresponding elemental mapping images of C, Co, Ni and O elements (Fig. 2e) demonstrated a well-defined core-shell structure of PANC@Co-Ni LDH. The lattice fringes of the nanoflakes exhibited interplane spacing of 0.25 nm,

View Article Online
DOI: 10.1039/C8SE00123E

corresponding to the (012) plane of Co-Ni LDH, as shown in Fig. 2f FFT image of PANC@LDH sample, which is in great agreement with the XRD and XPS results (The high quality HRTEM is provided in Fig. S7). This special core-shell structures of PANC@Co-Ni LDH materials will reach its full potential of the good conductivity of core-like PANC and high specific capacitance of shell-like Co-Ni LDH[35,36].

Electrochemical characterization of Negative electrode materials

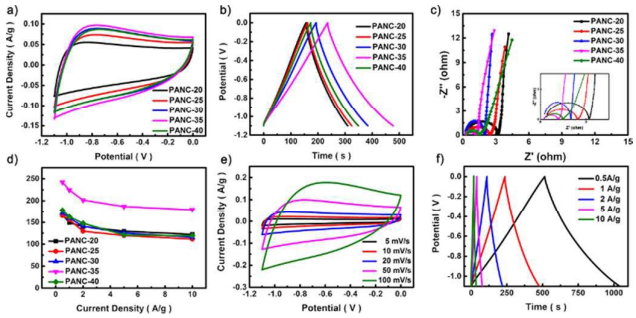

Fig. 3 (a) CV curves of the various PANC-x at a scan rate of 50 mV s^{-1}; (b) GCD curves of the various PANC-x at a current density of 1 A g^{-1}; (c) Nyquist plots of PANC-x. Inset is the magnification of Warburg semicircles from the spectra; (d) The specific capacitance of the PANC-x at different current densities; (e) CV curves of the PANC-35 at various scan rates; (f) GCD curves of the PANC-35 at different current densities.

The electrochemical behavior of the PANC-x electrodes were systematically measured in a three-electrode configuration using 6 M KOH as electrolyte. Fig. 3a-3c showed the cyclic voltammograms (CV), galvanostatic discharge-charge (GCD) profiles and Nyquist plots of the PANC-x. No redox peaks appearing in the CV curves revealed its carbon materials based electrical double-layer capacitors (EDLCs) types. The smallest close areal in CV curves, the longest discharge time at the same current density together with the lowest Rct (resistance of charge-transfer=1.46 Ω) of the PANC-35 sample demonstrated that 35 cycles is the most optimal electrodeposition cycles, which is in accordance with aforementioned SEM and XRD results. The specific capacitance of PANC-x (Fig. 3d) intuitively proved the best performance of the PANC-35, which shows the largest specific capacitance of 224.26 F g^{-1} among all of PANC-x samples (PANC-20 167.12 F g^{-1}; PANC-25 165.18 F g^{-1}; PANC-30 171.4 F g^{-1}; PANC-40 178.05 F g^{-1}), corresponding to the results of CV measurements. The CV curves of PANC-35 at different scan rate were measured, as displayed in Fig. 3e. The rectangular shapes of the CV curves of PANC-35 electrode were still retained at scan rates varying from 5 to 100 mV s^{-1}, demonstrating the excellent rate properties. From the GCD curves of PANC-35 at different current densities (Fig. 3d), we can see that there is no obvious voltage drop even at high current of 10 A g^{-1}, which means the little equivalent series resistance. The calculated specific capacitance based on the GCD curves showed an excellent capacitance retention of 74.1% when current densities improved 20 times. The comparison of the specific capacitance of various N-doped carbon material in three-electrode system revealed the high capacitance of the PANC-35 samples, as shown in Table S1. The excellent electrochemical properties of PANC-35 is mainly attributed to its unique porous nanostructures and self N-doped carbon component, more specifically, 1) the opening hierarchical porous nanowires could stimulate ions in electrolyte transport over the entire surface of the PANC; 2) the PANC nanowires as a self N-doped carbonaceous supported skeleton with outstanding electrical conductivity, facilitate electron transport could enhance its rate performance; 3) The self N-doped carbon could ameliorate the wettability and electrochemical activity, resulting in the further improvement of the specific capacitance.[4,38]

PANC@LDH: Positive electrode material

To determine the most effective electrodeposition time (T) for Co-Ni LDH-T, a series of comparison experiments were carried out at first, as shown in Fig. 4a-4d. The CV curves of the LDH@CFP showed a pair of strong redox peaks, indicating that the capacitance characteristics are mainly provided by Faradaic redox reactions. Fig. 4b displayed the CV curves of the PANC@LDH-T (T= 100, 200, 300 and 400 s) in 6 M KOH aqueous at a scan rate of 4 mV s^{-1}. It's obvious that shell-like Co-Ni LDH-300 coted PANC NWs reached a maximum close areal compared to others, which also demonstrated by the longest charge time and the highest specific capacitance of 1529.52 F g^{-1} (Fig 4c and 4d). The capacitance decreased significantly with the deposition time rising to 400s might be explained by the excessive deposition of LDH, the reduction of the electrochemical activity and unaccomplished redox reaction of Co-Ni LDH. The final mass loading of the PANC@LDH-300 hybrid electrode was weighed to be 13.4 mg (Fig. S6).

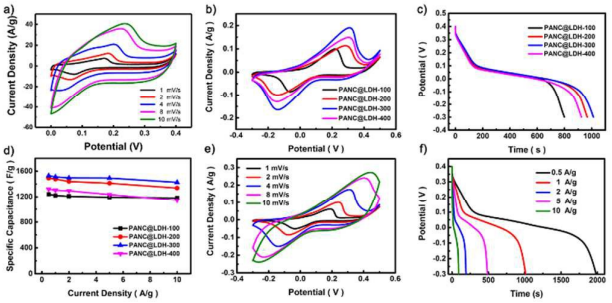

Fig. 4 (a) CV curves of the LDH@CFP (b) CV curves of the PANC@LDH-T (T=100, 200, 300 and 400s) at a scan rate of 4 mV s^{-1}; (c) GCD curves and the specific capacitance of the PANC@LDH-T at different current densities; (e) CV curves of the PANC@LDH-300 at various scan rates; (f) GCD curves of the PANC@LDH-300at different current densities.

Fig. 4e showed the CV curves of the PANC@LDH-300 at different scan rate varying from 1 to 10 mV s^{-1}. Obvious redox peaks were observed from the CV curves. However, when the scan rate increases from 1 to 10 mV s^{-1}, the redox peaks shifted gradually and got less distinct due to are the fast-insufficient redox reactions and the polarization effect of the PANC@LDH-300 electrode. Fig. 4f displayed the corresponding GCD profiles of various PANC@LDH-T samples in a potential window ranging from -0.3 to 0.4 V, the platforms confirmed

View Article Online
DOI: 10.1039/C8SE00123E

the redox process. On the basis of GCD curves, the specific capacitance of the electrode was calculated and the capacitance retention of 93.17% was obtained, suggesting the excellent rate performance of the PANC@Co-Ni LDH-300 electrode. Table S2 showed the electrochemical performance comparison of LDH-300@PANC with the LDHs in previous reports, which revealed that the PANC@Co-Ni LDH-300 is also competitive electrode materials for SCs. These excellent performances of the PANC@Co-Ni LDH-300 electrode can be accounted by the following reasons. Firstly, the self N-doped PANC NWs with good wettability and conductivity enables Co-Ni LDH nanoflakes to deposit and Co-Ni LDH have large open surface, which could improve the utilization efficiency of electrode. Secondly, core-shell structure of PANC@Co-Ni LDH shortens the electron transport distance and reduces the charge transfer resistance.[34,39] Thirdly, the good interfacial contact between the Co-Ni LDH and PANC NWs greatly lowers the internal resistance of electrode.[18]

LDH@PANC//PANC: Asymmetric supercapacitor device

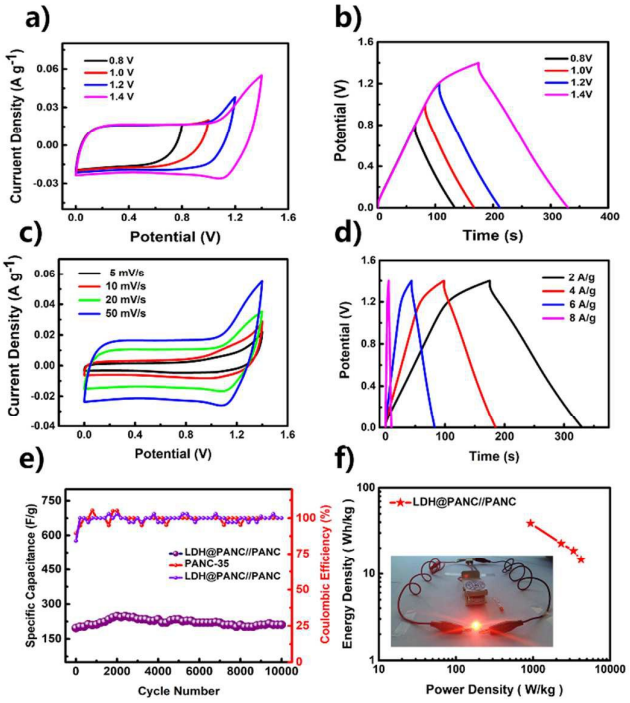

Fig. 5 (a) CV curves and (b) GCD curves of the PANC@LDH //PANC ASC with different working voltage windows; (c, d) CV and GCD curves of the fabricated ASC devices; (e) Cycling stability of PANC@LDH //PANC ASC at current density of 2 A g^{-1} and corresponding Coulombic efficiency; (f) Ragone plots of the PANC@LDH //PANC ASC, the inset is the photographs of LED indicator powered by two tandem connected ASC devices.

To evaluate the practical application of the synthesized electrode materials, an ASC was fabricated using PANC@Co-Ni LDH-300 as positive electrode and PANC-35 as negative electrode. Fig. 5a and 5b depicted the CV and GCD curves of the fabricated devices, which realize the improvement of the potential windows. Fig. 5c presented its CV curves at various scan rates from 5 to 50 mV s^{-1} under a wide potential window of 0-1.4 V. It can be seen that the similar rectangular shape with no obvious redox peaks of CV curves as the scan rate increased, which indicates the quick I-V response and high reversible energy storage ability. The specific capacitance of the ASC device calculated by the GCD curves (Fig. 5d), are 214.28 F g^{-1}, 200.83 F g^{-1},178.98 F g^{-1} and 152.36 F g^{-1}, corresponding to the current density of 2, 4, 6 8 A g^{-1}. The relatively higher specific capacitance can be proved by the Table S3. The cyclic performance also is an important factor to evaluate SCs, therefore, the long-term cyclic stabilities of as-assembled ASC were tested at a current density of 2 A g^{-1} for 10,000 cycles, as shown in Fig. 5e. Almost 84.73% (211.25 F g^{-1}) of the initial capacitance (249.23 F g^{-1}) retained after 10,000 cycles, showing outstanding cycle properties. The maximum energy density and power density of the ASC device were calculated as 38.73 W h kg^{-1} (0.92 kW kg^{-1}) and 4.2 kW kg^{-1} (14.01 W h kg^{-1}), which is much higher than that of traditional AC//AC SCs (~10 W h kg^{-1}) and previously reported ASC devices listed in Table S3. As a visualized demonstration for practical application, a red light-emitting diode (LED) was easily lit up by two ASCs connected in series for about 10 minutes (the inset of Fig. 5f), conforming that our devices can be used as a portable energy storage.

Conclusions

In summary, a novel core-shell PANC@Co-Ni LDH electrode materials was successfully synthesized by facile electrochemical deposition and carbonization method. Owing to the good conductivity of the self N-doped PANC structures and high theoretical specific capacitance of the Co-Ni LDH nanoflakes, the fabricated PANC@Co-Ni LDH//PANC ASC delivered a high specific capacitance of 214.28 F g^{-1} with a wide potential window of 1.4V, excellent cycling stability with 85.17% of the initial capacitance attenuation after 10,000 cycles and a high energy density of 38.73Wh kg^{-1} at power density of 0.92 kW kg^{-1}. Such good results provide a powerful candidate for advanced electrode materials.

Acknowledgements

The authors sincerely acknowledge financial support from National Natural Science Foundation of China (NSFC Grant Nos. 21571080) and Natural Science Foundation of Jilin province (No. 20170101193JC)

Notes and references

1. L. Li, Z. Lou, D. Chen, K. Jiang, W. Han and G. Shen, *Small*, 2017 2829.
2. W. Li, D. Chen, Z. Li, Y. Shi, Y. Wan, J. Huang, J. Yang, D. Zhao and Z.Jiang, *Electrochem. Commun.*, 2007, **9**, 569-573.
3. M. R. Lukatskaya, B. Dunn and Y. Gogotsi, *Nat. Commun.*, 2016, **7**,12647.
4. Y. Xi, G. Wei, J. Li, X. Liu, M. Pang, Y. Yang, Y. Ji, V. Y. Izotov,Q. Guo and W. Han, *Electrochim. Acta*, 2017, **233**, 26-35.
5. S. Zhong, C. Zhan and D. Cao, *Carbon*, 2015, **85**, 51-59.

View Article Online
DOI: 10.1039/C8SE00123E

6. D. Pech, M. Brunet, H. Durou, P. Huang, V. Mochalin, Y.Gogotsi,P.L. Taberna and P. Simon, *Nat. Nanotechnol.*, 2010, **5**, 651-654.
7. Y. Gogotsi, A. Nikitin, H. Ye, W. Zhou, J. E. Fischer, B. Yi, H. C.Foley and M. W. Barsoum, *Nat. Mater.*, 2003, **2**, 591-594.
8. M. Liu, B. Li, H. Zhou, C. Chen, Y. Liu and T. Liu, *Chem. Commun.* , 2017, **53**, 2810-2813.
9. M. Kim, C. Lee and J. Jang, *Adv. Funct. Mater.* , 2014,**24**, 2489-2499.
10. Y. Gawli, A. Banerjee, D. Dhakras, M. Deo, D. Bulani, P.Wadgaonkar, M. Shelke and S. Ogale, *Sci. Rep.*, 2016, **6**, 21002.
11. X. Xiao, H. Song, S. Lin, Y. Zhou, X. Zhan, Z. Hu, Q. Zhang, J.Sun, B.Yang, T. Li, L. Jiao, J. Zhou, J. Tang and Y. Gogotsi, *Nat. Commun.*, 2016, **7**, 11296.
12. M. A. Garakani, S. Abouali, Z.-L. Xu, J. Huang, J.-Q. Huang and J.-K.Kim, *J. Mater. Chem. A*, 2017, **5**, 3547-3557.
13. Z. Gu and X. Zhang, *J. Mater. Chem. A*, 2016, **4**,8249-8254.
14. Z. Gu, H. Nan, B. Geng and X. Zhang, *J. Mater. Chem. A*, 2015, **3**, 12069-12075.
15. Y. Qian, R. Liu, Q. Wang, J. Xu, D. Chen and G. Shen, *J. Mater. Chem. A*, 2014, **2**, 10917-10922.
16. R. R. Salunkhe, K. Jang, S.-w. Lee, S. Yu and H. Ahn, *J. Mater. Chem.*, 2012, **22**, 21630.
17. Z. Tang, C.-h. Tang and H. Gong, *Adv. Funct. Mater.*,2012, **22**, 1272-1278.
18. X. Li, J. Shen, W. Sun, X. Hong, R. Wang, X. Zhao and X. Yan, *J. Mater. Chem. A*, 2015, **3**, 13244-13253.
19. S. Zeng, H. Chen, F. Cai, Y. Kang, M. Chen and Q. Li, *J. Mater. Chem. A*, 2015, **3**, 23864-23870.
20. O. Mashtalir, M. Naguib, V. N. Mochalin, Y. Dall'Agnese, M. Heon,M. W. Barsoum and Y. Gogotsi, *Nat. Commun.* , 2013, **4**, 1716.
21. S. Xu, G. Wei, J. Li, W. Han and Y. Gogotsi, *J. Mater. Chem. A* , 2017, **5**, 17442-17451.
22. S. Xu, G. Wei, J. Li, Y. Ji, N. Klyui, V. Izotov and W. Han, *Chem. Eng. J.* , 2017, **317**, 1026-1036.
23. P. Singh and K. Pal, *Electrochim. Acta*, 2017, **242**, 47-55.
24. Z. Zhang, L. Wang, Y. Li, Y. Wang, J. Zhang, G. Guan, Z. Pan, G.Zheng and H. Peng, *Adv. Energy Mater.* , 2017, **7**, 1601814.
25. M. Radoičić, G. Ćirić-Marjanović, V. Spasojević, P. Ahrenkiel, M.Mitrić, T. Novaković and Z. Šaponjić, *Appl. Catal. B* , 2017, **213**, 155-166.
26. K. Kan, L. Wang, P. Yu, B. Jiang, K. Shi and H. Fu, *Nanoscale*, 2016,**8**, 10166-10176.
27. J. J. Langer and S. Golczak, *Polym. Degrad. and Stab.* , 2007, **92**, 330-334.
28. D.-s. Yuan, T.-x. Zhou, S.-l. Zhou, W.-j. Zou, S.-s. Mo and N.-n. Xia, *Electrochem. Commun.* , 2011, **13**, 242-246.
29. P. Hasin, V. Amornkitbamrung and N. Chanlek, *J. Catal.* , 2017, **351**, 19-32.
30. D. Du, X. Wu, S. Li, Y. Zhang, W. Xing, L. Li, Q. Xue, P. Bai and Z.Yan, *J. Mater. Chem. A*, 2017, **5**, 8964-8971.
31. Y. Chen, W. K. Pang, H. Bai, T. Zhou, Y. Liu, S. Li and Z. Guo, *Nano Lett.* , 2017, **17**, 429-436.
32. S. Liu, S. C. Lee, U. Patil, I. Shackery, S. Kang, K. Zhang, J. H. Park, K. Y. Chung and S. Chan Jun, *J. Mater. Chem. A* , 2017, **5**, 1043-1049.
33. Z. Yin, Y. Bu, J. Ren, S. Chen, D. Zhao, Y. Zou, S. Shen and D. Yang, *Chem. Eng. J.* , 2018, **03**, 100.
34. W. H. Choi, M. J. Choi and J. H. Bang, *ACS Appl. Mater. Interfaces.* , 2015, **7**, 19370-19381.
35. L. Zhang, T. You, T. Zhou, X. Zhou and F. Xu, *ACS Appl. Mater. Interfaces.* , 2016, **8**, 13918-13925.
36. Y. Zhu, J. Ren, X. Yang, G. Chang, Y. Bu, G. Wei, W. Han and D. Yang, *J. Mater. Chem. A, 2017, **5**, 9952* M. Shao, Z. Li, R.
37. X. Wang, S. Chen, D. Li, S. Sun, Z. Peng, S. Komarneni and D. Yang, *ACS Sustain. Chem. Eng. 2018, **6**, 633*
38. J. Cui, Y. Xi, S. Chen, D. Li, X. She, J. Sun, W. Han, D. Yang and S. Guo, *Adv. Funct. Mater.* , 2016, **26**, 8487-8495.
39. Zhang, F. Ning, M. Wei, D. G. Evans and X. Duan, *Small*, 2015, **11**, 3530-3538.